Viability of Mobius Topologies in [26]- and [28]Hexaphyrins

ARTICLE *in* CHEMISTRY - A EUROPEAN JOURNAL · JULY 2012

Impact Factor: 5.73 · DOI: 10.1002/chem.201200511 · Source: PubMed

3 AUTHORS, INCLUDING:

Mercedes Alonso
Vrije Universiteit Brussel
38 PUBLICATIONS **231** CITATIONS
SEE PROFILE

Paul Geerlings
Vrije Universiteit Brussel
460 PUBLICATIONS **11,521** CITATIONS
SEE PROFILE

CHEMISTRY
A EUROPEAN JOURNAL

ChemPubSoc
Europe

DOI: 10.1002/chem.201200511

Viability of Möbius Topologies in [26]- and [28]Hexaphyrins

Mercedes Alonso,* Paul Geerlings, and Frank de Proft[a]

Abstract: Recently, hexaphyrins have emerged as a promising class of π-conjugated molecules that display a range of interesting electronic, optical, and conformational properties, including the formation of stable Möbius aromatic systems. Besides the Möbius topology, hexaphyrins can adopt a variety of conformations with Hückel and twisted Hückel topologies, which can be interconverted under certain conditions. To determine the optimum conditions for viable Möbius topologies, the conformational preferences of [26]- and [28]hexaphyrins and the dynamic interconversion between the Möbius and Hückel topologies were investigated by density functional calculations. In the absence of *meso* substituents, [26]hexaphyrin prefers a planar dumbbell conformation, strongly aromatic and relatively strain free. The Möbius topology is highly improbable: the most stable tautomer is 33 kcal mol^{-1} higher in energy than the global minimum. On the other hand, the Möbius conformer of [28]hexaphyrin is only 6.5 kcal mol^{-1} higher in energy than the most stable dumbbell conformation. This marked difference is due to aromatic stabilization in the Möbius $4n$ electron macrocycle as opposed to antiaromatic destabilization in the $4n+2$ electron system, as revealed by several energetic, magnetic, structural, and reactivity indices of aromaticity. For [28]hexaphyrins, the computed activation barrier for interconversion between the Möbius aromatic and Hückel antiaromatic conformers ranges from 7.2 to 10.2 kcal mol^{-1}, in very good agreement with the available experimental data. The conformation of the hexaphyrin macrocycle is strongly dependent on oxidation state and solvent, and this feature creates a promising platform for the development of molecular switches.

Keywords: aromaticity · density functional calculations · Möbius structures · porphyrinoids · ring strain

Introduction

Expanded porphyrins, the higher homologues of porphyrins, have attracted considerable attention in the last decade due to their exceptional optical, electrochemical, and coordination properties.[1,2] The rich chemistry of expanded porphyrins has led to a diverse family of structures with applications as ion sensors,[3] near-infrared dyes,[4] two-photon absorption materials,[5] and nonlinear optical materials.[2b,6] In addition, these macrocycles are the most appropriate molecular systems to test the practical limits of the Hückel rule for aromaticity and antiaromaticity.[7] Aromaticity is one of the most widely used concepts in chemistry,[8] but the debate on a sharp definition has continued in the last two decades.[9,10] Nevertheless, aromaticity is often used to justify or even predict the stability and properties of organic[11] and inorganic compounds,[12] metal clusters,[13] nanomaterials,[14] and Möbius-type molecules,[15] which are appealing topological structures.

According to the well-known Hückel rule, an aromatic compound is a cyclic molecular structure stabilized by the delocalization of $4n+2$ π electrons, while cyclic compounds with $4n$ π electrons are antiaromatic and unstable. On the other hand, Möbius aromaticity predicts that the above $4n+2$ and $4n$ Hückel rule should be reversed for π systems that lie on a singly twisted Möbius topology.[16] Accordingly, conjugated cyclic molecules can be classified as Hückel or Möbius systems depending on the number of half-twists in the ring (or, more precisely, the linking number L_k).[17] Molecules with an even number of half-twists are predicted to follow the Hückel rule, whereas those with an odd number of half-twists (Möbius systems) follow the reverse Hückel rule. Figure 1 also shows the twisted Hückel topology, characterized by two half twists ($L_k=2$), which is equivalent to the figure-of-eight conformation found in certain expanded porphyrins.[18]

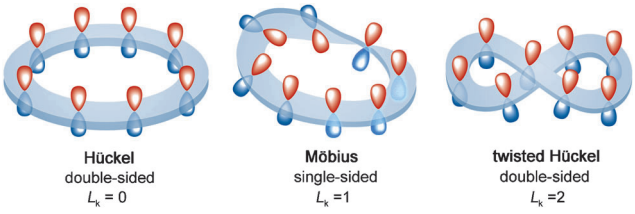

Figure 1. Schematic representation of the topologies of π-conjugated electron systems, adapted from Ref. [19].

[a] Dr. M. Alonso, Prof. P. Geerlings, Prof. F. de Proft
Eenheid Algemene Chemie (ALGC)
Vrije Universiteit Brussel (VUB)
Pleinlaan 2, 1050 Brussels (Belgium)
Fax: (+32) 2-6293317
E-mail: malonsog@vub.ac.be

Supporting information for this article is available on the WWW under http://dx.doi.org/10.1002/chem.201200511.

The intriguing concept of Möbius aromaticity was proposed in 1964 by Heilbronner,[20] and since then it was applied to possible transition states[21] and reactive intermediates.[22] However, the synthesis of a viable aromatic Möbius system was a challenge for 40 years until the seminal work of Herges et al. in 2003.[23] The difficulty of its synthesis resides in the implementation of two conflicting structural features, that is, cyclic full π conjugation and a singly twisted topology within a single molecule. In small macrocycles, the destabilization due to ring strain is larger than the stabilization due to Möbius aromaticity. To reduce this ring strain, large cyclic molecules can be envisaged, although the structures become more flexible, and they can flip back to the less-strained and viable Hückel topology.

The problem of the small *cis–trans* isomerization barriers for annulenic systems makes it difficult to synthesize stable Möbius conformers.[21b,24] However, it was recently shown that expanded porphyrins with more than five pyrrolic subunits can be used to solve this problem, by taking advantage of their conformational flexibility and the number and the nature of substituents on the pyrrolic and *meso* positions.[1] The first truly stable Möbius aromatic system was obtained by Osuka and co-workers, who introduced a new feature into these expanded porphyrins, namely, metalation of the macrocycle.[19]

Among porphyrinoids, hexaphyrins consisting of six pyrrolic units are emerging functional molecules in light of their conformational flexibility,[25] unique reactivities, diverse metalation behavior,[26] and extremely large two-photon absorption cross sections.[27,28] An attractive feature of hexaphyrins is their ability to adopt two stable oxidation states, corresponding to a 26π- and 28π-electron states, which can be easily interconverted by two-electron redox reactions.[29] Through extensive studies, it has been recognized that most *meso*-aryl [26]hexaphyrins adopt rectangular conformations, although other shapes, such as dumbbell, figure-of-eight, and triangular conformations, have also been identified, depending on the substituents and the external conditions.[30] The conformational preferences of [28]hexaphyrins are more complicated and, until 2008, it was not proven that Hückel and Möbius topologies coexist in solution at room temperature.[31,32]

Topology switching in expanded porphyrins can be achieved without breaking the ring. Such a change of topology is achieved through internal rotations and, if properly controlled, can provide access to molecular switches with unique optical and magnetic properties. Recently, a three-level topological change (planar Hückel, Möbius, and twisted Hückel) of A,D-di-*para*-benzo[28]hexaphyrin was shown to occur by temperature and acid/base control, providing a potentially versatile route to molecular devices.[33] Specifically, hexaphyrins are very promising platforms to develop new optical switches, since Möbius and Hückel conformers exhibit high values of and large differences in NLO properties.[28,25a]

Despite the extraordinary progress made in the chemistry of expanded porphyrins, many aspects and applications remain to be analyzed. Computational chemistry is a powerful tool in aiding the design of viable[34] Möbius aromatic systems, since it can provide a full description and comprehension of the Möbius aromaticity. The main aim of this work is to analyze the role of ring strain, hydrogen bonding, and aromaticity in the stability of Möbius and Hückel conformers of unsubstituted [26]- and [28]hexaphyrins by DFT.[35] In addition, the dynamic interconversion between the Hückel and Möbius topologies for the two stable oxidation states is also investigated theoretically, and the effect of the solvent and temperature is analyzed. Aromaticity is often described as a multidimensional phenomenon that can not be quantified by a single descriptor.[36] Accordingly, we employed a large set of aromaticity indices based on energetic, magnetic, structural, and reactivity criteria to quantify the aromaticity of these large macrocycles. The performance of the different indices in describing Möbius aromaticity is also analyzed.

Computational methods

All calculations were performed with the Gaussian 09 program suite[37] by using the three-parameter B3LYP functional[38] and 6-31G(d,p) basis set. The geometries of the different conformers and tautomers of the [26]- and [28]hexaphyrins ([26]HxP and [28]HxP) were fully optimized and characterized by harmonic vibrational frequency computations. All structures corresponded to minima on the potential-energy surface with no imaginary frequencies. The energies were corrected by B3LYP/631G-(d,p) zero-point energies.

The performance of the B3LYP hybrid functional on the geometries, relative conformational energies, and activation energy barriers of hexaphyrins was assessed by comparison with experiment. We also tested the BH&HLYP functional[39] and the recently developed meta M06-2X functional[40] with a large contribution of Hartree–Fock exchange, since they overcome most of the shortcomings of the B3LYP functional.[41] The geometries optimized with the different methods are similar, although B3LYP predicts more delocalized and bond length equalized structures than BH&HLYP and M06-2X. Interestingly, B3LYP bond lengths are in better agreement with X-ray values. There is no significant difference between the energies computed with M06-2X and B3LYP, except for the Möbius topology of [26]HxP. Furthermore, the activation barrier for the [28]HxP topological switch in gas phase and solvent is more accurately reproduced by the B3LYP functional. BH&HLYP should be avoided for studying hexaphyrins, since it underestimates the activation barrier and fails to reproduce correctly the stability of the Möbius conformer for the [28]HxP. Single-point calculations at the B3LYP/6-311+G(d,p) level of theory also showed that the influence of the basis sets is rather small. The results obtained with the different methods are reported in the Supporting Information.

The Hückel–Möbius interconversion pathway in hexaphyrins was followed by rotation of the internal dihedral angles φ_1 and φ_2 in the rectangular conformer (Scheme 1). The rotation of each *transoid meso* bridge is accompanied by rotation of the adjacent D pyrrole ring. The relaxed potential-energy surfaces, as respective functions of φ_1 or φ_2, were computed at the B3LYP/6-31G(d,p) level of theory; φ_1 and φ_2 were systematically varied from 180 to −180° with a step size of 10°. All local minima and transition states were further optimized without any geometrical restriction and verified by frequency calculations. For the transition states, only one imaginary frequency was found corresponding to D pyrrole rotation. IRC calculations from the transition states were performed for both sides of the reaction path. Implicit solvent effects were computed by using the polarizable continuum model (PCM) with radii and nonelectrostatic terms from Truhlar and co-workers' SMD model[42] at the B3LYP/631G-

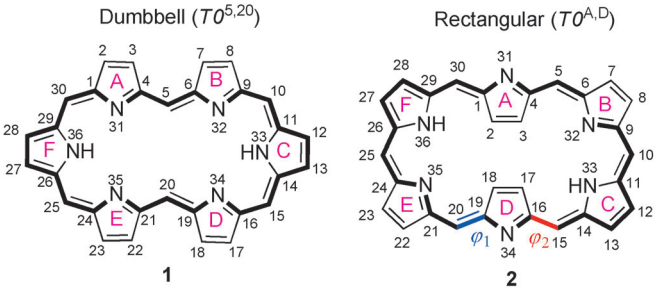

Scheme 1. Numbering of atoms in [26]hexaphyrins **1** and **2**. φ_1 and φ_2 are the two selected reaction coordinates for the Hückel–Möbius interconversion. The topological descriptor Tn^X indicates the number of half-twists (n), that is, linking number, and the subunits located between two *transoid* linkages (X).

(d,p) level of theory. The solvent effects were calculated at the gas-phase geometries to give a solvation-free energy.

The aromatic stabilization energies (ASEs) of the [26]- and [28]hexaphyrin conformers were evaluated by using the Schleyer–Pühlhofer isomerization method (ISE), which is based on the energy difference between a methyl derivative of the conjugated system and its nonaromatic exocyclic methylene isomer.[43] The ISE method is especially effective in evaluating the ASEs of highly strained systems and it has been applied to measure the ASEs of Hückel- and Möbius-type annulenes.[44] As a rule, the methyl group was placed on *meso* carbon atom 10, between pyrrole rings B and C. The reaction used to evaluate the isomerization stabilization energy of the dumbbell conformer **1** of [26]hexaphyrin is shown in Scheme 2. This method requires application of *syn–anti* corrections due

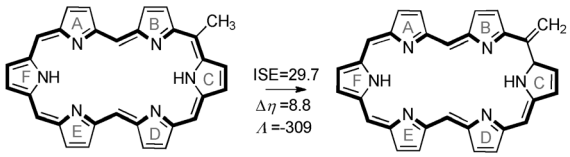

Scheme 2. Example of the isomerization reaction used to evaluate the isomerization stabilization energy (ISE), magnetic susceptibility exaltation Λ, and relative hardness $\Delta\eta$ of hexaphyrins. ISE and $\Delta\eta$ are given in kcal mol^{-1} and Λ in ppm cgs.

to the *cis–trans* diene mismatches in the methyl and methylene isomers.[43] The *syn–anti* corrections were evaluated as the energy difference between the dihydrogen derivative of the *meso*-methyl hexaphyrin and its respective nonaromatic isomer, as shown in Scheme 3 for **1**. Systems with positive ASE/ISE values are aromatic, whereas those with strongly negative ASE/ISE values are considered to be antiaromatic.

The magnetic susceptibility exaltation Λ and the nucleus independent chemical shift (NICS) were used as magnetic descriptors of aromaticity. The former is defined as the difference between the magnetic susceptibility of a compound χ_M and that of a reference compound without cyclic electron delocalization $\chi_{M'}$ [Eq. (1)].[45] The exaltations of hexaphyrins

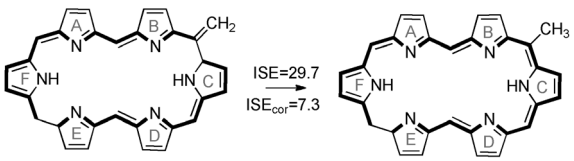

Scheme 3. *Syn–anti* correction for the ISE of **1**, computed by means of Scheme 2.

were obtained from the reaction indicated in Scheme 2, without application of the *syn–anti* correction. The magnetic susceptibilities were computed by the CSGT method[46] at the HF/6-31+G(dp) level of theory, as recommended by Cyrański et al.[47] The exaltations are negative (diamagnetic) for aromatic compounds and positive (paramagnetic) for antiaromatic compounds.

$$\Lambda = \chi_M - \chi_{M'} \quad (1)$$

The NICS is defined as the negative value of the absolute magnetic shielding computed at the ring center or another interesting point of the system.[48] The NICS(1) values, calculated 1 Å above the molecular plane, and the corresponding out-of-plane component of the NICS tensor, denoted NICS$_{zz}$(1), are considered to better reflect the π-electron effects in organic compounds such as [n]annulenes.[49] The GIAO/B3LYP/6-311+G(d,p) method was used for the NICS calculations. Rings with highly negative values of NICS are quantified as aromatic, whereas those with positive values are antiaromatic. NICS values were calculated at the geometrical center of the 36 heavy atoms of the hexaphyrin framework. NICS were also evaluated in the geometrical center of the heavy atoms belonging to the classical conjugation pathway (CP), but they are practically identical, and they are reported in the Supporting Information (Table S5).

As a structure-based descriptor, we employed the harmonic oscillator model of aromaticity (HOMA) defined by Kruszewski and Krygowski [Eq. (2)][50]

$$\mathrm{HOMA} = 1 - \frac{\alpha}{n}\sum_{i=1}(R_{opt} - R_i) \quad (2)$$

where n is the number of bonds taken into the summation, and α is an empirical constant fixed to give HOMA=0 for a model nonaromatic system and HOMA=1 for a system with all bonds equal to an optimal value R_{opt}, assumed to be realized for a fully aromatic system. R_i is the running bond length along the conjugation pathway.

The aromaticity analysis was complemented with the calculation of the relative hardness $\Delta\eta$ as a reactivity descriptor of the aromaticity. The concept of hardness can be linked to the aromatic character of cyclic π-electron systems, and especially the relative hardness, introduced by some of us, was shown to be a good measure of aromaticity for a series of five-membered C_4H_4X compounds.[51] The chemical hardness η is the resistance of the systems towards a change in its number of electrons.[52] Assuming a quadratic relation between E and N, the chemical hardness η can be calculated from the vertical ionization potential I and the vertical electron affinity A according to the finite difference approximation [Eq. (3)]

$$\eta = I - A \quad (3)$$

which, by using a Koopmans-type approximation,[53] becomes Equation 4.

$$\eta = \varepsilon_{LUMO} - \varepsilon_{HOMO} \quad (4)$$

The relative hardness $\Delta\eta$ was computed by the isomerization method. The LUMO and HOMO energies of the *meso*-methyl hexaphyrin and its respective nonaromatic methylene isomer were computed at the B3LYP/6-31G(d,p) level of theory.

Results and Discussion

Conformational analysis: Hexaphyrins(1.1.1.1.1.1) having six single-carbon *meso* bridges adopt a variety of structures depending on the peripheral substituents at the β and/or *meso* positions and the oxidation state. The conformational equilibria can be modulated by different chemical factors, such

as temperature, solvent, pH, metal coordination, and ring-fusion reactions.[1,25] Six main conformations were considered in our study: dumbbell (D), rectangular (R), figure-of-eight (F), triangular (T), hexagonal (H), and Möbius (M). Except for the hexagonal convex structure, these conformations have been identified experimentally for several all-aza-hexaphyrins. The three-dimensional structures of the major conformations of [26]hexaphyrins are shown in Figure 2.

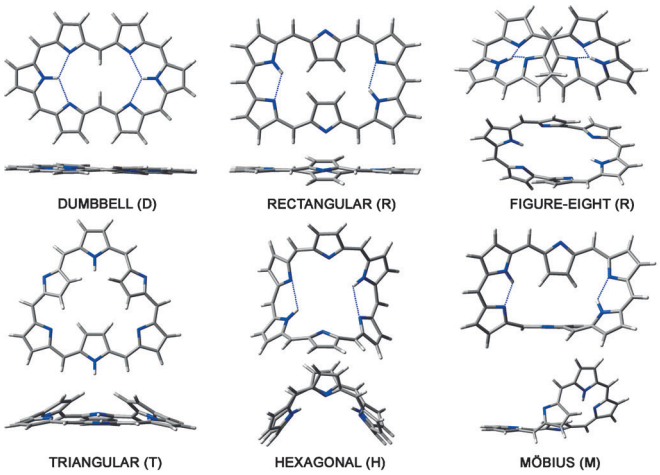

Figure 2. 3D structures (top and side views) of the main conformers of [26]hexaphyrin. The intramolecular hydrogen bonds are represented by blue dotted lines.

The stability of these conformers depends on the intramolecular hydrogen bonding inside the macrocycle, steric effects, ring strain, and π conjugation. The NH···N intramolecular hydrogen bonds in the Hückel and Möbius conformers of [26]hexaphyrin are depicted in the Figure 2. The hydrogen-bonding network inside the cavity is measured by the hydrogen bonding index N_H, which assigns a value of 1 for single NH···N bonds and 1.5 for bifurcated ones. For a series of regular and N-confused [26]hexaphyrins, it was recently shown that the stability of the NH tautomers in each Hückel conformation is governed by the N_H index, whereby one intramolecular hydrogen bond affords stabilization by about 10 kcal mol^{-1}.[54] In our conformational study on [26]- and [28]hexaphyrins, where possible, experimentally observed tautomers were chosen. In addition, different tautomers with similar N_H values for the Möbius topology and the Hückel conformations of [28]HxP were also investigated to test how tautomerism affects both the stability and aromaticity of the macrocyclic system. The conformations together with their corresponding tautomers of the [26]- and the [28]hexaphyrins included in the study are shown in Schemes 4 and 5.

Ring-strain energy is an important factor governing the relative energies in porphyrinoid macrocycles. Evaluation of the ring strain is based on the dihedral angles of the π-conjugated circuit. Two torsional parameters were calculated for the different conformations of [26]- and [28]hexaphyrins:

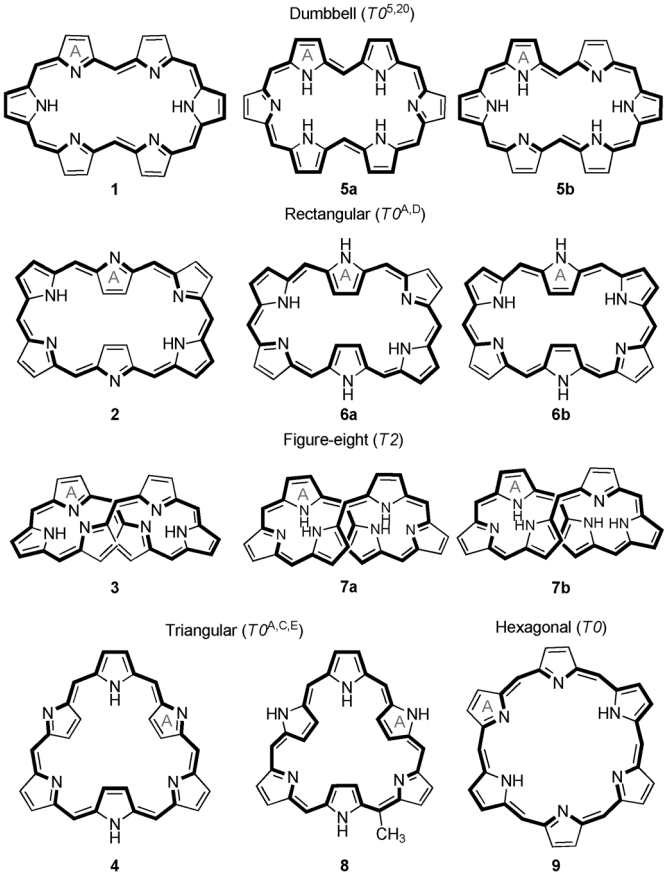

Scheme 4. Hückel conformations of [26]- and [28]hexaphyrins. For each conformation of the [28]annulenoid system, two tautomers were also included in the study. The classical conjugation pathway is depicted with bold bonds.

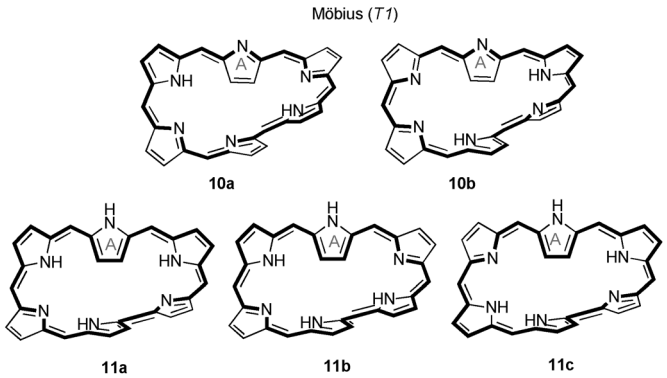

Scheme 5. Möbius conformers of [26]- and [28]hexaphyrins. Different tautomers with similar hydrogen-bonding index were also studied.

the average dihedral angle between neighboring pyrrole rings Φ_p[54] and the average absolute deviation from 0 or 180° of the dihedral angles ψ along the classical conjugation pathway (CP),[55] indicated by bold bonds in Schemes 4 and 5. In principle, conformations having small values of Φ_p and ψ would be favorable, since a strainless dipyrromethene unit takes on a planar conformation. It is remarkable that a very

good linear dependence between Φ_p and ψ is found, with a correlation coefficient $R^2=0.98$ (Supporting Information Figure S2). Therefore, we can use either of these two concepts for measuring the ring strain in hexaphyrins.

In addition, the reduced overlap of neighboring p orbitals is measured by the torsional π-conjugation index Π, defined by Stępień as follows [Eq. (5)][1b]

$$\Pi = \prod_i cos\phi_i \qquad (5)$$

where φ_i are the dihedral angles along the CP; $\Pi=1$ for a completely planar system, and it is positive for any Hückel (double-sided) surface regardless of its linking number; it tends to 0 for rings containing a torsion very close to $\pm 90°$; it is negative for any Möbius (single-sided) surface regardless of the linking number and it approaches -1 for infinitely large rings with uniformly distributed torsions. Small absolute values (typically smaller than 0.3) are characteristic of systems with no observable macrocyclic aromaticity.[1b] All of these torsional descriptors together with the relative energies of the [26]- and [28]hexaphyrin conformers and tautomers are collected in Table 1. The differences in length between the shortest and longest C–C and C–N bonds Δr are also included in Table 1, as a measure of bond-length alternation. On the basis of the geometrical parameters, one can assume that a higher degree of bond alternation and a larger deviation from planarity will correspond to a lower aromaticity. This issue is analyzed in detail further below.

Table 1. Relative energies E_{rel} [kcal mol^{-1}], hydrogen bonding index N_H, ring strain descriptors Φ_p and ψ [°], torsional π-conjugation index Π, and bond-length alternation Δr_{C-N} and Δr_{C-C} [Å] of the main conformations/tautomers of [26]- and [28]hexaphyrins.

Compound	Conf	E_{rel}[a]	N_H	Φ_p	ψ	Π	Δr_{C-N}	Δr_{C-C}
[26]hexaphyrin								
1	D	0.00	3	3.70	1.03	0.99	0.007	0.065
2	R	10.05	2	11.91	3.80	0.91	0.006	0.065
3	F	24.06	3	31.30	9.37	0.58	0.007	0.064
4	T	35.40	0	24.07	8.25	0.65	0.040	0.087
9	H	48.16	2	45.69	16.72	0.21	0.008	0.061
10a	M	33.00	2	32.16	10.07	−0.36	0.081	0.101
10b	M	35.95	2	34.20	11.72	−0.39	0.082	0.100
[28]hexaphyrin								
5a	D	0.00	3	10.69	3.02	0.87	0.048	0.097
5b	D	5.59	2	9.90	2.61	0.92	0.053	0.095
6a	R	9.24	2	11.40	3.44	0.90	0.055	0.090
6b	R	9.35	2	11.49	3.46	0.90	0.055	0.091
7a	F	12.32	3	31.51	10.46	0.40	0.047	0.096
7b	F	16.24	2.5	31.27	10.42	0.43	0.047	0.091
8	T	34.01	0	22.33	6.66	0.70	0.054	0.096
11a	M	6.45	2.5	32.10	9.87	−0.51	0.011	0.066
11b	M	7.60	2.5	32.29	10.37	−0.45	0.009	0.062
11c	M	8.87	2	31.32	9.83	−0.50	0.005	0.062

[a] Evaluated at the B3LYP/6-31G** level of theory including zero-point energy.

For unsubstituted [26]hexaphyrin, the global energy minimum corresponds to dumbbell conformation **1**, which is stabilized by two bifurcated NH···N hydrogen bonds and is relatively strain-free with the smallest values of Φ_p and ψ. This planar Hückel conformation is preferred for *meso*-aryl [26]HxP lacking aryl groups at the 5- and 20-positions[56] or bearing small 2-thienyl or 3-thienyl substituents at these *meso* positions.[30b] The presence of bulky substituents at the inward *meso* positions substantially increases the steric repulsion, forcing a conformational change to a rectangular conformation, in which the pyrrole rings A and D are inverted. The rectangular conformer **2** is predicted to be 10 kcal mol^{-1} less stable than the dumbbell conformer **1** for unsubstituted [26]HxP, largely due to the loss of two "half" hydrogen bonds. Conformer **2** is roughly planar with an average dihedral angle along the CP of 3.8°. The high values of Π suggest that macrocyclic conjugation may be quite effective in both Hückel conformations.

The other three Hückel conformations (figure-of-eight **3**, triangular **4**, and hexagonal **9**) are much less stable, with energy differences with respect to D conformer **1** of 24, 35, and 48 kcal mol^{-1}, respectively. Despite the four intramolecular hydrogen bonds, the high ring strain imposed by the two formal half-twists in the π system of **3** means that the figure-of-eight or lemniscular conformation cannot be easily located for [26]HxP. X-ray diffraction analysis revealed a double-twisted F conformation for *meso*-trifluoromethyl-substituted [26]- and [28]HxP.[57] A topological analysis on these hexapyrrolic compounds showed that half of the twisting strain is compensated by adopting this lemniscular conformation with similar amount of twist (T_w) and writhe (W_r).[58] The triangular conformation **4** is quite rare for [26]HxP and only can be achieved by making the molecule C_3-symmetric, which is achieved by the introduction of three alternate confused pyrrole rings or on protonation with methanesulfonic acid.[59] The inverted rings A and E in **4** strongly deviate from the macrocyclic plane (Figure 1), with an angle between the two mean planes of 32°. However, macrocyclic conjugation should be effective, since $\Pi=0.65$. The ring strain is highly increased in convex conformer **9**, in which all subunits have a *cis–cis* alignment. According to $\Pi=0.2$, the macrocyclic conjugation is quite ineffective in this highly nonplanar conformation.

The Möbius topology is highly improbable for [26]HxP: the most stable tautomer **10a** is 33 kcal mol^{-1} higher in energy than the dumbbell conformer. The singly twisted *T1* conformers exhibit significant bond-length alternation ($\Delta r_{C-C}=0.1$ Å), in agreement with their expected antiaromatic character according to the reversed Hückel rules. The Π parameter range of -0.36 to -0.39 suggests that the π overlap should be efficient in both *T1* tautomers. The energy difference of 3 kcal mol^{-1} between **10a** and **10b** is mainly due the higher ring strain and the longer hydrogen-bond lengths in the latter.

The relative stability of Möbius conformers is quite different for the [28]hexaphyrins. At the B3LYP/6-31G** level of theory, the experimental tautomer **11a** is only 6.45 kcal mol^{-1} higher in energy than the most stable dumbbell conformation **5a**. The average C–C distance in **11a** is 1.41 Å

and it exhibits smaller bond alternation ($\Delta r_{c-c}=0.07$ Å) than the rest of the Hückel conformations. Both Φ_p and ψ predict similar ring strains for the Möbius conformations of [26]- and [28]HxP, so the higher stability of **11a** is mainly due to the expected aromatic stabilization in the Möbius $4n$ electron system. In addition, three hydrogen bonds stabilize **11a**, but only two such interactions are found in **5a**.

In **11a**, the large strain arising from the molecular twist is dissipated across the whole macrocyclic ring system, and the overlap of the π orbitals along the CP is quite effective ($\Pi=-0.51$). For example, the Möbius conformer of the regular porphyrin is a transition state and it is predicted to be 63 kcal mol^{-1} higher in energy than the convex conformer. The molecular twist significantly increases the ring strain ($\Phi_p=49.5$ and $\psi=14.7$) of the [18]annulenoid system and π conjugation is rather inefficient ($\Pi=-0.17$, Supporting Information Figure S2).

Interestingly, the global minimum corresponds to Hückel dumbbell conformation **5a** despite of its antiaromatic character. The six inward-oriented hydrogen atoms cause a loss of planarity in this Hückel conformation compared to [26]HxP. In spite of their high stability, *meso*-aryl [28]hexaphyrins exhibit a planar rectangular or a Möbius conformation, and only recently was a dumbbell shape characterized for radical and singlet biradical forms of *meso*-keto and diketo hexaphyrins.[60] The rectangular conformation **6a** is, however 2.8 kcal mol^{-1} less stable than Möbius conformer **11a**. This small energy difference can explain why *meso*-aryl-substituted [28]HxP exists in solution as an equilibrium of several equivalent twisted Möbius conformations and a Hückel rectangular conformation (Scheme 6). Depending on the temperature and the crystallization conditions, *meso*-aryl substituted [28]HxP preferably adopt a planar or singly twisted topology.[31,32]

The figure-of-eight conformation **7a** is 12.3 kcal mol^{-1} less stable than the most stable dumbbell conformer. This means that the lemniscular conformations should be more accessible for [28]HxP than for [26]HxP, in spite of its antiaromaticity. The triangular conformation is quite destabilized in both oxidation states. No stable minimum could be found for the 28-electron *T0* conformation. Optimization of this conformer led to the *T2* figure-of-eight conformation **7a**, which reduces the high ring strain imposed by the *cis–cis* arrangements.

The relative energies among the tautomers in each conformation of [28]HxP are mainly governed by the hydrogen-bonding interactions, since they have very similar ring strain and also similar degrees of aromaticity/antiaromaticity (see below). The most stable NH tautomer in each conformer corresponds to the experimental one.

Dynamic switching between Hückel and Möbius topologies in [26]- and [28]hexaphyrins: One of the most appealing applications of hexaphyrins is the possibility to switch between Möbius and Hückel topologies with different electronic structures and properties by applying only small changes in external conditions (temperature, solvent, pH) or ring structure (*meso* substituent, metal). Accordingly, we investigated theoretically the dynamic interconversion between the Hückel and Möbius topologies for [26]- and [28]HxP, identifying the transition states and evaluating the conformational barriers in the gas phase and in different solvents.

In porphyrinoids, it is possible to switch between different π-conjugation topologies without breaking the macrocyclic ring. This is achieved by variation of internal torsional angles and is the basis of a special type of aromaticity switching.[1b] While the macrocycle is preserved during the switching process, the π system can be said to be temporarily broken when one torsion angle becomes exactly ±90°. The simplest conversion pathway between the Hückel rectangular topology (*T0*^{A,D}, in which the pyrrole rings A and D are located between two *transoid* linkages) and the Möbius topology *T1* corresponds to the rotation of one of the *transoid* bonds. If one linkage is distorted enough to adopt a *cisoid* configuration ($90<\varphi<0°$), one obtains the singly twisted Möbius conformer (Scheme 7).

Two equivalent Möbius conformations can be obtained depending on which linkage of the rectangular conformation is rotated (φ_1 and φ_2 in Scheme 7). To assess how the energy

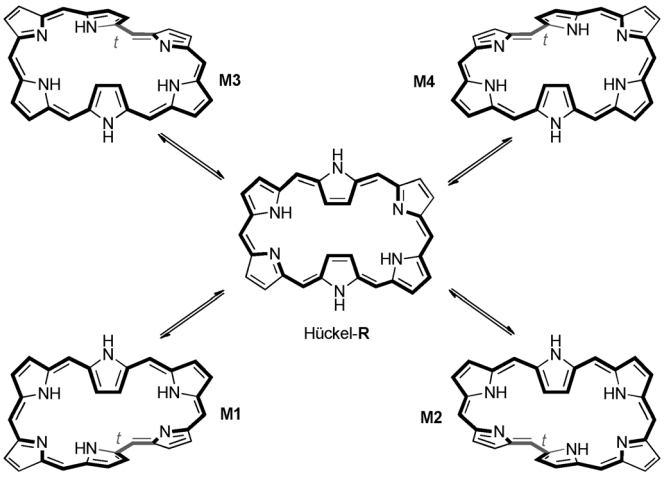

Scheme 6. Conformational equilibrium of *meso*-aryl [28]hexaphyrins, proposed in ref. [31]. *meso*-Aryl substituents are not shown. If all the *meso* positions bear the same aryl group, **M1** is identical to **M4** and **M2** is identical to **M3**, and these two pairs are enantiomeric.

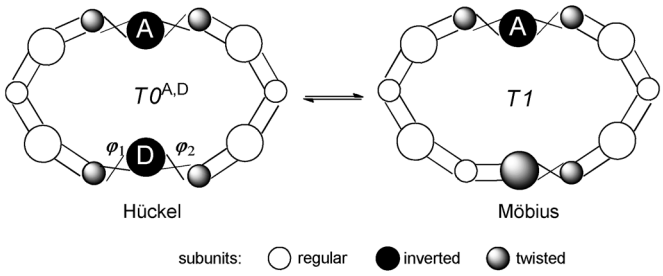

Scheme 7. Hückel–Möbius interconversion pathway in hexaphyrins. Big circles correspond to the pyrrole rings and small circles to the single-carbon *meso* bridges. Crossed lines denoted *transoid* linkages.

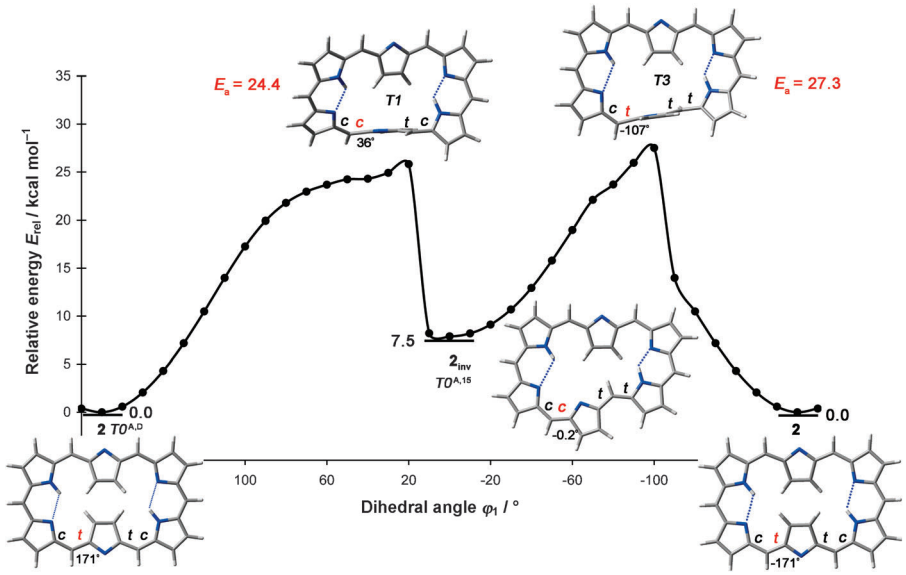

Figure 3. Potential-energy curve for the Hückel–Möbius interconversion in [26]HxP as a function of torsion angle φ_1. The fully optimized geometries for the minima and transition states and their corresponding relative energies with respect to the global minimum **2** are also shown.

varies with the rotation of each of the *trans* bonds, a relaxed potential-energy surface scan was performed at the B3LYP/6-31G** level of theory. The energy profile for φ_1 rotation in rectangular conformer **2** is depicted in Figure 3. The fully optimized geometries for the minima and transition states are also shown. The *cis* and *trans* geometry around four bonds is also depicted in Figure 3. The *cis* and *trans* geometry is defined by absolute torsion angles of $|\varphi_1| < 90°$ and $|\varphi_1| > 90°$, respectively, with respect to the smallest macrocyclic circuit (SMC), which is defined as the smallest circuit in the molecular graph passing through all subunits. As a result of the rotation of φ_1, a *tt*-aligned pyrrole ring is transformed into a *ct*-aligned subunit, and the number of *trans* bonds in the SMC decreases by one. The energy decreases drastically at 20°, but this energy drop remains present with smaller step sizes.

For the [26]HxP, the preferred conformation corresponds to the rectangular conformer **2**, and the Möbius *T1* topology (with an odd number of *trans* bonds) is a transition state in the topological switching. The associated activation energy is fairly large (E_a = 24.4 kcal mol^{-1}), which is consistent with the fact that no experimental example of a Möbius structure for the [26]annulenoid system has been found hitherto. Although the *T1* conformers **10a** (φ_1 = 13.8°) and **10b** (φ_1 = 15.4°) are local minima with no imaginary frequencies, the system strongly prefers a Hückel $T0^{A,15}$ conformation ($\mathbf{2_{inv}}$), which is only 7.5 kcal mol^{-1} less stable than the rectangular conformer. This D-inverted conformer $\mathbf{2_{inv}}$ is nearly planar (Φ_p = 8.5 and ψ = 3.24, Π = 0.92) and should be aromatic according to the Hückel rule.

A similar energy profile was found for rotation of the *transoid* bond φ_2 (see Figure S4 in the Supporting Information), although the inverted $T0^{A,20}$ conformer is only 0.55 kcal mol^{-1} higher in energy than **2** and the activation barrier is 20.8 kcal mol^{-1} (Scheme 8). For the regular porphyrin, inversion of a pyrrole ring ($T0 \rightarrow T0^A$) requires a much higher activation energy (E_A = 49.1 kcal mol^{-1}) and the inverted conformer is thermodynamically much less stable than the convex structure (E_{rel} = 44.3 kcal mol^{-1}). In this case, the *T1* Möbius topology was also considered as an alternative transition state in the pyrrole inversion $T0 \rightarrow T0^A$.[61] All these data confirm the high conformational flexibility present in the hexapyrrolic macrocycles compared to the tetrapyrrolic systems.

For the [28]HxP, there are two possible Hückel–Möbius interconversion paths depending on which tautomer is involved: **6a**→**11b** or **6b**→**11a**. According to the relative energies of the NH tautomers for the rectangular and Möbius conformations in Table 1, it should be energetically more favorable to perform the **6b**→**11a** interconversion. The energy profile for the φ_1 rotation in the $T0^{A,D}$ rectangular conformer **6b** is depicted in Figure 4.

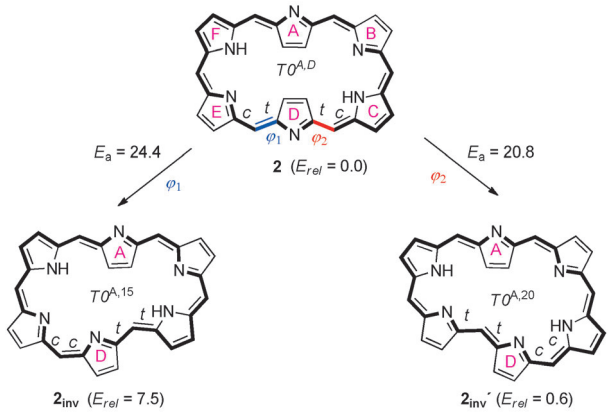

Scheme 8. Activation energy barriers [kcal mol^{-1}] for conformational switch in [26]HxP by rotation of dihedral angle φ_1 or φ_2, respectively.

The potential-energy curve obtained for the [28]annulenoid system is completely different from that of [26]HxP. The preferred conformation is the singly twisted Möbius topology **11a**, and the rectangular conformation **6b** is 2.9 kcal mol^{-1} higher in energy. The activation barrier for the Hückel-Möbius conformational interconversion is predicted to be only 9.9 kcal mol^{-1} in the gas phase, which is in good agreement with the spectroscopically derived activation bar-

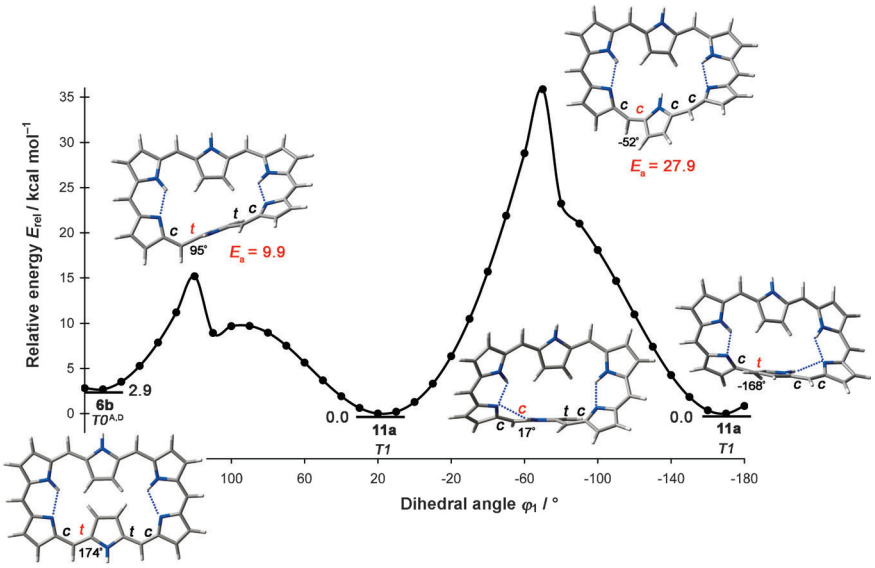

Figure 4. Potential-energy curve for the Hückel–Möbius interconversion in [28]HxP as a function of dihedral angle φ_1. The fully optimized geometries for the minima and transition states and their corresponding relative energies with respect to the global minimum **11a** are also shown.

rier of 8 ± 1 kcal mol^{-1} for *meso*-hexakis(pentafluorophenyl) [28]HxP.[32,62] The activation energy barrier decreases from 9.91 to 8.78 kcal mol^{-1} at the B3LYP/6-311+G(d,p) level of theory (Supporting Information Table S2). In the transition state φ_1 becomes 95° and the π system is temporarily broken ($\Pi = -0.06$). The hydrogen-bonding interactions in **6b** are conserved along the whole reaction pathway and increase in the single-sided topology. The low activation energy barrier and the small energy difference between the planar and Möbius conformations of [28]HxP mean that both conformers easily and rapidly interconvert at room temperature, and are predominantly the *T1* structures. A similar energy profile is found for interconversion between Hückel tautomer **6a** and Möbius tautomer **11b** (Supporting Information Figures S6 and S7). The activation energy barrier is 10.1 kcal mol^{-1}, and $\varphi_1 = 93°$ in the transition state.

The effect of temperature and solvent on the Hückel–Möbius topological switch of the [28]HxP was also analyzed theoretically. The corresponding Gibbs free energies ΔG calculated at 298 K and 173 K are collected in Table 2. At the lowest temperature, the Möbius conformer is indeed more favored thermodynamically, with ΔG of the planar conformation increased by 0.3 kcal mol^{-1}. The ^{1}H NMR spectrum of *meso*-hexakis(pentafluorophenyl) [28]HxP at 173 K showed that the conformational equilibrium is frozen at this temperature, so that a single Möbius conformer is detected.[31]

The free solvation energies of **6a**, **6b**, **11a**, and the transition state (**TS**) were calculated by using the recently introduced solvation model SMD[42] at the B3LYP/6-31G(d,p) level of theory. This is the recommended model for computing ΔG of solvation and it has been parametrized with a training set of 2821 solvation data. The solvation energies in *n*-hexane, *n*-heptane, $CHCl_3$, THF, CH_2Cl_2, EtOH, MeOH, DMSO, and H_2O are collected in Table 2. Different mixtures of these solvents were employed in the crystallization process of several *meso*-aryl [28]HxP. Interestingly, *meso*-aryl [28]HxP provided two different X-ray crystal structures—a planar rectangular conformation or a Möbius one—depending on the solvents used for crystallization.[31]

Table 2 shows that the solvent plays an important role in the conformational stability of unsubstituted [28]HxP. As the dielectric constant of the solvent increases, the Hückel rectangular tautomers become more stable, and **6a** is the global minimum in MeOH, DMSO, and H_2O. The activation energy barrier also diminishes in polar solvents. In fact, the solid-state structure of *meso*-hexakis(C_6F_5) [28]HxP obtained from DMSO/methanol/H_2O corresponds to the rectangular structure, in which the two outward-pointing NH protons are hydrogen-bonded to two solvent DMSO molecules. In apolar solvents, such as *n*-heptane, *n*-hexane, and chloroform, the Möbius conformation is favored. Most of the solid-state Möbius structures were obtained by using binary mixtures of nonpolar solvents such as $CHCl_3$/*n*-hexane and THF/*n*-heptane. On the other hand, most of the X-ray rectangular structures of [28]HxP were crystallized from solvent mixtures comprising a polar solvent like THF/methanol, $CHCl_3$/methanol, or CH_2Cl_2/*n*-heptane.[63]

Table 2. Gibbs free energies ΔG [kcal mol^{-1}] for the Hückel–Möbius topological switch in [28]HxP calculated at 298 and 173 K and in different solvents.

Comp	Conf	298 K	173 K	*n*-hexane	*n*-heptane	$CHCl_3$	THF	CH_2Cl_2	EtOH	MeOH	DMSO	H_2O
ε[a]				1.88	1.91	4.71	7.43	8.93	24.85	32.61	46.83	78.36
6a	R	2.23	2.56	1.70	1.68	0.37	0.05	0.00	0.00	0.00	0.00	0.00
6b	R	2.33	2.67	1.83	1.81	0.50	0.17	0.12	0.12	0.12	0.12	0.13
11a	M	0.00	0.00	0.00	0.00	0.00	0.00	0.13	0.78	0.90	0.64	2.33
TS10.24		10.24	10.03	9.16	9.14	7.78	7.46	7.36	7.24	7.22	7.31	7.45

[a] Dielectric constant of the solvent.

Aromaticity of the Hückel and Möbius conformations of [26]- and [28]hexaphyrins: In recent years, numerous methods to quantify aromaticity based on the energetic, magnetic, structural, and electronic properties have been proposed, but none of them is universal. Conse-

quently, aromaticity analyses should employ a set of aromaticity descriptors based on different physical manifestations of aromaticity. In this regard, aromaticity of hexaphyrins has been quantified by using several energetic, structural, magnetic, and reactivity criteria. HOMA and NICS have been applied extensively to describe Möbius aromaticity, but it is important to assess the performance of the different indices for describing Möbius aromaticity, since the introduction of curvature can induce large variations in the calculated values. We preclude using electronic indices such as the multicenter indices[64] or the aromatic fluctuation index,[65] since their high computational cost is a drawback for their evaluation in large systems. In addition, the value of the multicenter index strongly depends on the number of centers, decreasing dramatically as n increases.[66] So, for the large 26- and 28-center rings it is expected that the multicenter index will tend to 0.

Table 3. Calculated uncorrected and *syn–anti*-corrected stabilization energies (ISE and ISE_{corr} [kcal mol^{-1}]), Λ [ppm cgs], $\Delta\eta$ [kcal mol^{-1}], NICS and $NICS_{zz}(1)$ [ppm], and HOMA for [26]- and [28]hexaphyrins.

Comp	Conf	ISE	ISE_{corr}	Λ	$\Delta\eta$	NICS	$NICS_{zz}(1)$	HOMA
benzene		34.4	34.3	−18	55.3	−8.0	−29.2	0.982
1	D	29.7	7.3	−309	8.79	−14.8	−38.1	0.874
2	R	31.7	7.4	−400	7.06	−17.7	−35.8	0.877
3	F	22.9	6.0	−118	3.84	−12.1	−24.5	0.847
4	T	23.7	4.7	−335	2.51	−12.3	−28.9	0.819
9	H	−1.2[a]	1.8	−159	2.42	−9.7	−26.4	0.882
10a	M	13.9	−3.4	146	−5.43	5.8	27.1	0.656
10b	M	15.3	−2.9	231	−4.92	10.6	41.7	0.671
5a	D	20.7	−3.5	805	−11.36	37.6	107.3	0.683
5b	D	21.5	−4.0	796	−12.05	37.9	106.5	0.696
6a	R	19.8	−4.8	1019	−11.85	47.1	136.9	0.706
6b	R	19.6	−10.3[b]	1042	−11.45	47.9	139.0	0.705
7a	F	19.4	−3.5	177	−10.30	10.4	38.6	0.644
7b	F	16.8	−4.3	199	−11.61	10.9	41.4	0.666
8	T	17.9	−3.6	655	−11.72	28.2	82.7	0.671
11a	M	22.8	1.7[b]	−221	9.14	−14.9	−27.4	0.819
11b	M	21.6	6.0	−216	7.22	−14.7	−27.4	0.824
11c	M	23.6	5.5	−195	7.17	−14.9	−29.0	0.829

[a] Optimization of the methylene isomer led to a minimum with two half-twists (*T2)*, which does not resemble the hexagonal conformation (*T0*) of the methyl derivative. [b] The *syn–anti* corrections for tautomers **6b** and **11a** are overestimated because the dihydrogen methylene isomers are less stable than that of **6a** and **11b** and **11c**, respectively (see Supporting Information).

Two of the most frequently used aromaticity descriptors, namely, the aromatic stabilization energy (ASE) and the magnetic susceptibility exaltation Λ, depend strongly on the reference systems. Devising a convenient reaction scheme for large and flexible expanded porphyrins such as hexaphyrins is not an easy task. The energies derived from the different schemes may be perturbed by additional effects such as strain, unbalanced *syn–anti* interactions, hybridization, and heteroatom interactions like anomeric effects, hyperconjugation, and so on, which contaminate the estimated ASE values.[67] In this work, we applied the isomerization stabilization energy method (ISE) for evaluating the ASE, Λ, and the relative hardness $\Delta\eta$ of the [26]- and [28]hexaphyrins. The ISE method involves comparison of the total energies, magnetic susceptibilities, and hardnesses of only two species: a methyl derivative of the cyclic conjugated system and its nonaromatic exocyclic methylene isomer (Scheme 2). As a single closely related reference compound is involved, ISE should minimize perturbing effects such as strain. On the basis of this scheme, systems with positive ASE/ISE values are aromatic, whereas those with strongly negative ASEs are considered to be antiaromatic. The aromatic isomerization energies computed at the B3LYP/6-31G(d,p) level, together with the rest of the aromaticity descriptors, are collected in Table 3. The aromaticity descriptors of benzene, the prototypical aromatic compound, are also included for comparison.

The ISE value computed at the same level of theory for benzene is 34.4 kcal mol^{-1}, in close agreement with the most recent reliable estimate of its stabilization energy of approximately 32 kcal mol^{-1}.[68] However, the uncorrected ISE values are positive for all Hückel and Möbius conformations of the [26] and [28]HxP, except for hexagonal conformer **9**. In this highly strained conformation, the optimized geometry of the methylene isomer corresponds to a doubly twisted conformation *T2*, which does not resemble the *T0* structure obtained for the methyl derivative (Supporting Information Figure S11). The high positive ISE values are mainly due to the unbalanced *syn–anti* diene conformations on both sides of the reaction scheme. The importance of the *syn–anti* corrections was realized for antiaromatic [4*n*]annulenes; thus, the ISE of [24]annulene decreased from 18 to −2.4 kcal mol^{-1} after the correction was applied.[44b] In the ISE method *syn–anti* corrections are evaluated by employing the dihydrogen derivative of the methyl-hexaphyrin and its nonaromatic isomer as conjugated reference species (Scheme 3).[69] The corrected ISE values (ISE_{corr}) are listed in Table 3. ISE_{corr} is an energetic measure of the global aromaticity of hexaphyrins.[70]

For [26]HxP, the overall stabilization gained through the cyclic delocalization of $4n+2$ π electrons is predicted to be around 7.4 kcal mol^{-1} in the dumbbell and the rectangular conformations. Since both conformers have essentially the same degree of aromaticity, the conformational interconversion between **1** and **2** is controlled by the interplay between the intramolecular hydrogen bonding and the steric effects of the *meso* substituents. The highest ISE_{corr} values correspond to the more planar conformers **1** and **2**, although the figure-of-eight conformation **3** ($\Phi_p = 31.3°$) with $ISE_{corr} =$ 6 kcal mol^{-1} is more aromatic than triangular structure **4** ($\Phi_p = 24.1°$), and consequently it is more stable. In agreement with Heilbronner's prediction, the Möbius [26]HxP conformers **10a** and **10b** are destabilized, but only to

a small extent ($ISE_{corr} \approx -3$ kcal mol^{-1}). The ISE_{corr} values suggest that the degree of macrocyclic aromaticity for the [26]HxP conformers decreases in the order: rectangular ≈ dumbbell > figure-of-eight > triangular > hexagonal > Möbius. It is remarkable that the effect of the aromatic stabilization is significantly less pronounced for the large hexaphyrins than for smaller monocycles such as benzene ($ISE_{corr} = 34.3$ kcal mol^{-1}).

A reverse aromaticity order is found for the [28]hexaphyrin conformations. All of the Hückel conformations are slightly destabilized by π-electron delocalization and characterized by negative ISE_{corr} values, ranging from −4.8 to −3.5 kcal mol^{-1}. However, the destabilizing effects in the large [28]annulenoid system are small, and accordingly the presence of the antiaromatic rectangular conformer is observable in both solution and solid state. [28]Hexaphyrin is stabilized by adopting a twisted single-sided topology with Möbius aromaticity. The positive ISE_{corr} values of the Möbius conformations indicate the presence of macrocyclic aromaticity.

The isomerization method has been also employed for evaluating Λ and the relative hardness $\Delta\eta$ of hexaphyrins **1**–**11** (Table 3). The Λ value was proposed as the major criterion of the aromaticity, since it is the only measurable property which is uniquely associated with aromaticity.[10b] However, as energetic criterion, Λ is strongly dependent on the reaction scheme. Interestingly, the Λ value derived from the ISE equation correlates very well with the different NICS descriptors for the studied hexaphyrins. The square of the correlation coefficient (R^2) of 0.987 indicates a very good linear dependence between all of the magnetic indices (Figure 5). The mutual relationships between magnetic aromaticity indices strongly depend on the selection of molecules in the sample, and some magnetic characteristics themselves may be orthogonal to others.[71] Furthermore, the excellent correlations between the different NICS-based indices indicate that the isotropic NICS values computed at the geometrical center of the hexaphyrin framework can be used as a reliable descriptor of the degree of aromaticity/antiaromaticity of the different conformers/tautomers of the [26]- and [28]-hexaphyrins. In such large macrocycles, the influences of the σ system and from all three principal components of the NICS tensor are insignificant, unlike what happens in small [*n*]annulenes.[49]

All magnetic descriptors indicate that the Hückel conformations of the [26]hexaphyrins exhibit a strong diatropic ring current, and the strongest ring currents are found in the dumbbell and rectangular conformers **1** and **2**. The magnetic susceptibility exaltation and, to a lesser extent NICS, depends heavily on the ring area, and consequently the diatropic ring current sustained by figure-of-eight conformation **3** is weaker than those exhibited by the other the Hückel conformers, despite its larger energetic stabilization. Aihara recently showed that the intensity of the current induced in a given circuit is proportional to the aromatic stabilization energy arising from the circuit multiplied by the area of the circuit.[72]

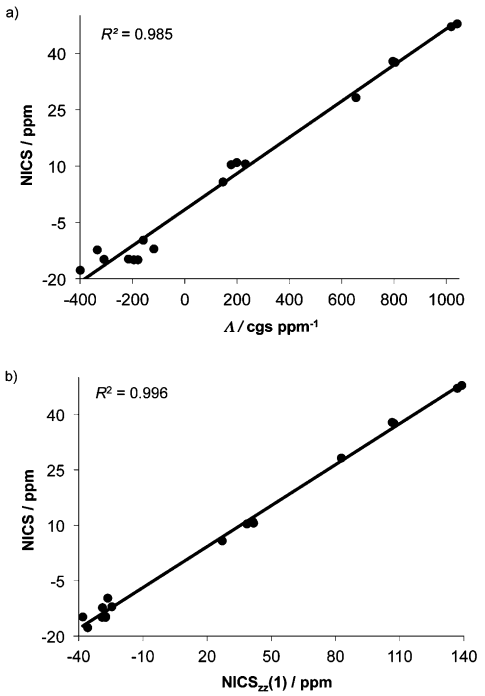

Figure 5. a) Correlation between the magnetic susceptibility exaltation Λ, computed by the isomerization method, and the isotropic NICS for the studied hexaphyrins. b) Correlation between the out-of-plane component of the NICS tensor computed at 1 Å [$NICS_{zz}(1)$] and the isotropic value computed at the geometrical center of the hexaphyrin framework [NICS].

Möbius [26]hexaphyrin conformers **10a** and **10b** exhibit paramagnetic susceptibility exaltation and have positive NICS values. The most intense paramagnetic ring current is found in the least stable tautomer **10b**. On the contrary, the Möbius conformers of the [28]HxP are diatropic and a very similar current strength is found in the tautomers **11a**, **11b**, and **11c**. The presence of intense paratropic ring currents in the dumbbell, rectangular, and triangular conformers of the [28]HxP is confirmed by the magnetic descriptors, which are significantly weaker in figure-of-eight conformation **7**.

The relative hardness $\Delta\eta$ of the hexaphyrins computed by the isomerization method is listed in Table 3. In the past, large bandgaps were associated with stable structures. This finding is nicely captured in the maximum hardness principle, which states that "molecules will arrange themselves to be as hard as possible".[70] According to the maximum hardness principle, the methyl derivative is expected to be systematically harder than the methylene isomer in the aromatic compounds, and vice versa in the antiaromatic systems. From the $\Delta\eta$ values listed in Table 2, all diatropic and paratropic conformations have positive and negative relative hardness, respectively. On the basis of $\Delta\eta$, [26]HxP prefers a dumbbell or rectangular conformation, while [28]HxP prefers a singly twisted conformation. The correlation coefficients R between the $\Delta\eta$ and the energetic, magnetic, and structural indices of aromaticity for the hexaphyrins studied in this work are listed in Table 4. In general, $\Delta\eta$ correlates well with the aromaticity descriptors, although they are

Table 4. Correlation coefficients between several descriptors of aromaticity for unsubstituted hexaphyrins ($n=18$).[a]

	ISE	ISE_{corr}	Λ	$\Delta\eta$	NICS	NICS(1)	$NICS_{zz}(1)$	HOMA
ISE	1							
ISE_{corr}	0.790[b]	1						
Λ	−0.515	−0.846[b]	1					
$\Delta\eta$	0.676	0.967[b]	−0.880[b]	1				
NICS	−0.505	−0.870[b]	0.993[b]	−0.908[b]	1			
NICS(1)	−0.505	−0.868[b]	0.993[b]	−0.905[b]	1.000[b]	1		
$NICS_{zz}(1)$	−0.530	−0.878[b]	0.992[b]	−0.908[b]	0.998[b]	0.999[b]	1	
HOMA	0.855[b]	0.926[b]	−0.728[b]	0.895[b]	−0.753[b]	−0.757[b]	−0.772[b]	1

[a] The correlations of ISE were calculated with omission of hexagonal conformer **9**, and the those of ISE_{corr} with omission of the tautomers **6b** and **11a**. [b] Correlation is significant at the 0.01 level (two-tailed).

based on different physicochemical properties. Therefore, we conclude that the relative hardness provides a simple and readily calculated measure of the global aromaticity of hexaphyrins.

The worst correlations are found for the structural parameter HOMA with the magnetic descriptors. HOMA predicts correctly that the Hückel conformers are more aromatic than the Möbius structures for the [26]HxP, although the HOMA values along the classical conjugation pathway (CP) for the antiaromatic **10a** and **10b** is about 0.66, a large value compared to other antiaromatic systems like the cyclopentadienyl cation (HOMA = −1.152).[36b] For the [28]HxP, the differences in the HOMA values between the aromatic Möbius conformer **11a** (HOMA = 0.829) and the antiaromatic rectangular conformer (HOMA = 0.706) are very small. As Herges previously observed for [16]annulenes,[15b] the Hückel [28]HxP conformers that exhibit a larger bond equalization have stronger paratropic ring currents and thus more antiaromatic magnetic properties (Supporting Information Figure S14). However, for the [26]HxP and the Möbius topologies, the correlation between HOMA and the magnetic indices is much better, so the conformers which exhibit larger negative NICS have larger HOMA values as expected.

In summary, the different energetic, magnetic, structural, and reactivity descriptors are correlated and distinguish between aromatic and antiaromatic hexaphyrins in a roughly similar way. However, for some conformations, such as the figure-of-eight conformations, the indices based on different physicochemical properties give contradictory trends. This is indicative of the multidimensional character of the aromaticity, and therefore the use of a single descriptor for quantifying the aromaticity of the hexaphyrins should be avoided. Application of a neural network for measuring the aromaticity of porphyrinoids and annulenes taking into account the main aromaticity descriptors is planned in further studies.

Conclusion

A thorough quantum chemical study of [26]- and [28]hexaphyrins focusing on the conformational preferences, dynamic topological switching, solvent effects, ring strain, and aromaticity has been reported. Six main conformations of hexaphyrins with Hückel, Möbius, and twisted-Hückel topologies have been investigated at the B3LYP/6-31G(d,p) level of theory. B3LYP shows the best overall performance for describing the geometries, thermochemistry, and kinetics of both oxidation states. M06-2X yielded very similar results. The results of this work lead us to the following conclusions:

The conformation of the hexaphyrin macrocycle is strongly dependent on the oxidation state and the aromatic versus antiaromatic character of the π-electron system. Although the most stable conformer corresponds to the less strained dumbbell-shaped conformation for unsubstituted [26]- and [28]hexaphyrin, the Möbius topology turns out to be indeed accessible for the $4n$ electron system. Interestingly, the figure-of-eight conformation is more easily achievable for [28]hexaphyrin in spite of its antiaromaticity.

While the relative stabilities of the [26]hexaphyrin conformers are mainly governed by ring strain (see Figure S16 in the Supporting Information), the aromatic stabilization controls the stability of the Möbius topologies. Hydrogen bonding is the main factor governing the relative stabilities of the NH tautomers in each conformation.

Topology switching is only achievable in [28]hexaphyrins. The Hückel antiaromatic and the Möbius aromatic conformers exist in conformational equilibrium and the activation energy barrier ranges from 7.2 to 10.2 kcal mol^{-1}. This equilibrium is quite sensitive to solvent; the Hückel rectangular conformation is more stable than the Möbius one in polar solvents.

The hexapyrrolic macrocycles benefit from a higher conformational flexibility than the tetrapyrrolic systems. The high ring strain imposed by the molecular twist in the regular porphyrin results in the Möbius conformer being 63 kcal mol^{-1} higher in energy than the planar one.

The aromaticity of the different conformers has been quantified using numerous descriptors of aromaticity, including energetic, magnetic, structural, and reactivity criteria. The isomerization method proved to be an effective method for evaluating ASEs (with application of the *syn–anti* corrections), magnetic susceptibility exaltation Λ, and relative hardness $\Delta\eta$ of hexaphyrins. In general good correlations exist between the different criteria, although some discrepancies are found. All hexaphyrin conformers with diatropic and paratropic ring currents have positive and negative ASEs and $\Delta\eta$, respectively. However, only the energetic, reactivity, and structural indices reveal that the aromaticity effect in such large macrocycles is much smaller than in benzene.

Our computational results support the experimental evidence available for [26]- and [28]hexaphyrins and thus show

how computational chemistry could be a powerful tool in aiding the design of viable Möbius aromatic systems and molecular switches. The torsional parameters Φ_p and ψ, π-conjugation index Π, and aromaticity indices are useful for identifying porphyrinoids with an optimum balance between the ring strain imposed by the macrocyclic core and energy stabilization due to aromatic conjugation. Interestingly, the nonlinear optical properties of porphyrinoids are closely related to the aromaticity and the molecular geometry. The computational methodology used in this work will therefore be applied in the near future to different porphyrinoids, such us pentaphyrins and heptaphyrins, in order to identify the most promising molecular materials.

Acknowledgements

M.A. thanks the European Community for financial support through the postdoctoral fellowship FP7-PEOPLE-2010-IEF-273527. P.G. and F.D.P thank the Fund for Scientific Research-Flanders (FWO) and the Free University of Brussels (VUB) for continuous support to their group.

[1] For excellent recent reviews, see: a) S. Saito, A. Osuka, *Angew. Chem.* **2011**, *123*, 4432–4464; *Angew. Chem. Int. Ed.* **2011**, *50*, 4342–4373; b) M. Stępień, N. Sprutta, L. Latos-Grażyński, *Angew. Chem.* **2011**, *123*, 4376–4430; *Angew. Chem. Int. Ed.* **2011**, *50*, 4288–4340.

[2] a) Z. S. Yoon, A. Osuka, D. Kim, *Nature Chem.* **2009**, *1*, 113–122; b) J. Y. Shin, K. S. Kim, M. C. Yoon, J. M. Lim, Z. S. Yoon, A. Osuka, D. Kim, *Chem. Soc. Rev.* **2010**, *39*, 2751–2767; c) J. L. Sessler, D. Seidel, *Angew. Chem.* **2003**, *115*, 5292–5333; *Angew. Chem. Int. Ed.* **2003**, *42*, 5134–5175.

[3] B. M. Rambo, J. L. Sessler, *Chem. Eur. J.* **2011**, *17*, 4946–4959.

[4] Y. Ikawa, M. Takeda, M. Suzuki, A. Osuka, H. Furuta, *Chem. Commun.* **2010**, *46*, 5689–5691.

[5] M. O. Pawlicki, H. A. Collins, R. G. Denning, H. L. Anderson, *Angew. Chem.* **2009**, *121*, 3292–3316; *Angew. Chem. Int. Ed.* **2009**, *48*, 3244–3266.

[6] a) J. M. Lim, Z. S. Yoon, J. Y. Shin, K. S. Kim, M. C. Yoon, D. Kim, *Chem. Commun.* **2009**, 261–273; b) M. C. Yoon, S. Cho, M. Suzuki, A. Osuka, D. Kim, *J. Am. Chem. Soc.* **2009**, *131*, 7360–7367.

[7] A. Osuka, S. Saito, *Chem. Commun.* **2011**, *47*, 4330–4339.

[8] a) P. J. Garrat, *Aromaticity*, John Wiley & Sons, New York, **1986**; b) V. I. Minkin, M. N. Glukhovtsev, B. Y. Simkin, *Aromaticity and Antiaromaticity: Electronic and Structural Aspects*, Wiley, New York, **1994**; c) T. M. Krygowski, M. K. Cyrański, Z. Czarnocki, G. Hafelinger, A. R. Katritzky, *Tetrahedron* **2000**, *56*, 1783–1796.

[9] In the last decade, *Chemical Reviews* has devoted two issues to the concept of aromaticity and its applications: a) *Chem. Rev.* **2001**, *101*, 1115–1566; b) *Chem. Rev.* **2005**, *110*, 3433–3947.

[10] a) A. Stanger, *Chem. Commun.* **2009**, 1939–1947; A sharp definition of aromaticity was provided in b) P. von Ragué Schleyer, H. J. Jiao, *Pure Appl. Chem.* **1996**, *68*, 209–218.

[11] a) A. T. Balaban, D. C. Oniciu, A. R. Katritzky, *Chem. Rev.* **2004**, *104*, 2777–2812; b) M. Alonso, B. Herradón, *J. Comput. Chem.* **2010**, *31*, 917–928.

[12] a) Z. Chen, R. B. King, *Chem. Rev.* **2005**, *105*, 3613–3642; b) Q. Zhang, S. Yue, X. Lu, Z. Chen, R. Huang, L. Zheng, P. von Ragué Schleyer, *J. Am. Chem. Soc.* **2009**, *131*, 9789–9799; c) M. J. Edward, *Coord. Chem. Rev.* **2011**, *255*, 2746–2763.

[13] For some reviews see: a) V. Y. Lee, A. Sekiguchi, *Angew. Chem.* **2007**, *119*, 6716–6740; *Angew. Chem. Int. Ed.* **2007**, *46*, 6596–6620; b) A. Sergeeva, B. Averkiev, A. Boldyrev, *Struct. Bonding (Berlin)* **2010**, 275–305.

[14] a) X. Lu, Z. Chen, *Chem. Rev.* **2005**, *105*, 3643–3696; b) F. J. Martín-Martínez, S. Melchor, J. A. Dobado, *Phys. Chem. Chem. Phys.* **2011**, *13*, 12844–12857.

[15] a) H. S. Rzepa, *Chem. Rev.* **2005**, *105*, 3697–3715; b) R. Herges, *Chem. Rev.* **2006**, *106*, 4820–4842.

[16] N. Jux, *Angew. Chem.* **2008**, *120*, 2577–2581; *Angew. Chem. Int. Ed.* **2008**, *47*, 2543–2546.

[17] The linking number L_k is an integer value that corresponds to the number of half-twists formally applied to the ribbon. L_k consists of the twisting number T_w and the nonlocal writhing number W_r ($L_k = T_w + W_r$). T_w refers to the sum of the local torsions, while W_r is related to the strain of the molecular ring: S. M. Rappaport, H. S. Rzepa, *J. Am. Chem. Soc.* **2008**, *130*, 7613–7619.

[18] a) M. Stępień, L. Latos-Grażyński, N. Sprutta, P. Chwalisz, L. Szterenberg, *Angew. Chem.* **2007**, *119*, 8015–8019; *Angew. Chem. Int. Ed.* **2007**, *46*, 7869–7873; b) H. Hinrichs, A. J. Boydston, P. G. Jones, K. Hess, R. Herges, M. M. Haley, H. Hopf, *Chem. Eur. J.* **2006**, *12*, 7103–7115.

[19] Y. Tanaka, S. Saito, S. Mori, N. Aratani, H. Shinokubo, N. Shibata, Y. Higuchi, Z. S. Yoon, K. S. Kim, S. B. Noh, J. K. Park, D. Kim, A. Osuka, *Angew. Chem.* **2008**, *120*, 693–696; *Angew. Chem. Int. Ed.* **2008**, *47*, 681–684.

[20] E. Heilbronner, *Tetrahedron Lett.* **1964**, *5*, 1923–1928.

[21] a) H. E. Zimmerman, *J. Am. Chem. Soc.* **1966**, *88*, 1564–1565; b) C. Castro, W. L. Karney, M. A. Valencia, C. M. H. Vu, R. P. Pemberton, *J. Am. Chem. Soc.* **2005**, *127*, 9704–9705; c) J. F. Moll, R. P. Pemberton, M. G. Gutierrez, C. Castro, W. L. Karney, *J. Am. Chem. Soc.* **2007**, *129*, 274–275.

[22] a) M. Mauksch, V. Gogonea, H. Jiao, P. von Ragué Schleyer, *Angew. Chem.* **1998**, *110*, 2515–2517; *Angew. Chem. Int. Ed.* **1998**, *37*, 2395–2397; b) G. Bucher, S. Grimme, R. Huenerbein, A. A. Auer, E. Mucke, F. Köhler, J. Siegwarth, R. Herges, *Angew. Chem.* **2009**, *121*, 10156–10159; *Angew. Chem. Int. Ed.* **2009**, *48*, 9971–9974.

[23] D. Ajami, O. Oeckler, A. Simon, R. Herges, *Nature* **2003**, *426*, 819–821.

[24] a) A. R. Mohebbi, E. K. Mucke, G. R. Schaller, F. Köhler, F. D. Sönnichsen, L. Ernst, C. Näther, R. Herges, *Chem. Eur. J.* **2010**, *16*, 7767–7772; b) E. L. Spitler, C. A. Johnson, M. M. Haley, *Chem. Rev.* **2006**, *106*, 5344–5386.

[25] a) M. C. Yoon, P. Kim, H. Yoo, S. Shimizu, T. Koide, S. Tokuji, S. Saito, A. Osuka, D. Kim, *J. Phys. Chem. B* **2011**, *115*, 14928–14937; b) J. M. Lim, M. Inoue, Y. M. Sung, M. Suzuki, T. Higashino, A. Osuka, D. Kim, *Chem. Commun.* **2011**, *47*, 3960–3962; c) T. Koide, K. Youfu, S. Saito, A. Osuka, *Chem. Commun.* **2009**, 6047–6049.

[26] a) S. Shimizu, A. Osuka, *Eur. J. Inorg. Chem.* **2006**, 1319–1335; b) T. Tanaka, T. Sugita, S. Tokuji, S. Saito, A. Osuka, *Angew. Chem.* **2010**, *122*, 6769–6771; *Angew. Chem. Int. Ed.* **2010**, *49*, 6619–6621.

[27] Z. S. Yoon, J. H. Kwon, M. C. Yoon, M. K. Koh, S. B. Noh, J. L. Sessler, J. T. Lee, D. Seidel, A. Aguilar, S. Shimizu, M. Suzuki, A. Osuka, D. Kim, *J. Am. Chem. Soc.* **2006**, *128*, 14128–14134.

[28] T. K. Ahn, J. H. Kwon, D. Y. Kim, D. W. Cho, D. H. Jeong, S. K. Kim, M. Suzuki, S. Shimizu, A. Osuka, D. Kim, *J. Am. Chem. Soc.* **2005**, *127*, 12856–12861.

[29] S. Mori, K. S. Kim, Z. S. Yoon, S. B. Noh, D. Kim, A. Osuka, *J. Am. Chem. Soc.* **2007**, *129*, 11344–11345.

[30] a) S. Shimizu, J. Y. Shin, H. Furuta, R. Ismael, A. Osuka, *Angew. Chem.* **2003**, *115*, 82–86; *Angew. Chem. Int. Ed.* **2003**, *42*, 78–82; b) M. Suzuki, A. Osuka, *Chem. Eur. J.* **2007**, *13*, 196–202; c) M. Suzuki, A. Osuka, *Org. Lett.* **2003**, *5*, 3943–3946.

[31] J. Sankar, S. Mori, S. Saito, H. Rath, M. Suzuki, Y. Inokuma, H. Shinokubo, K. Suk Kim, Z. S. Yoon, J. Y. Shin, J. M. Lim, Y. Matsuzaki, O. Matsushita, A. Muranaka, N. Kobayashi, D. Kim, A. Osuka, *J. Am. Chem. Soc.* **2008**, *130*, 13568–13579.

[32] K. S. Kim, Z. S. Yoon, A. B. Ricks, J.-Y. Shin, S. Mori, J. Sankar, S. Saito, Y. M. Jung, M. R. Wasielewski, A. Osuka, D. Kim, *J. Phys. Chem. A* **2009**, *113*, 4498–4506.

[33] M. Stępień, M. Szyszko, L. Latos-Grażyński, *J. Am. Chem. Soc.* **2010**, *132*, 3140–3152.

[34] R. Hoffmann, P. von Ragué Schleyer, H. F. Schaefer III, *Angew. Chem.* **2008**, *120*, 7276–7279; *Angew. Chem. Int. Ed.* **2008**, *47*, 7164–7167.
[35] W. Koch, M. C. Holthausen, *A Chemist's Guide to Density Functional Theory*, Wiley-VCH, Weinheim, **2000**.
[36] a) A. R. Katritzky, K. Jug, D. C. Oniciu, *Chem. Rev.* **2001**, *101*, 1421–1449; b) M. Alonso, B. Herradón, *Phys. Chem. Chem. Phys.* **2010**, *12*, 1305–1317.
[37] Gaussian 09, Revision B.01, M. J. Frisch, G. W. Trucks, H. B. Schlegel, G. E. Scuseria, M. A. Robb, J. R. Cheeseman, G. Scalmani, V. Barone, B. Mennucci, G. A. Petersson, H. Nakatsuji, M. Caricato, X. Li, H. P. Hratchian, A. F. Izmaylov, J. Bloino, G. Zheng, J. L. Sonnenberg, M. Hada, M. Ehara, K. Toyota, R. Fukuda, J. Hasegawa, M. Ishida, T. Nakajima, Y. Honda, O. Kitao, H. Nakai, T. Vreven, J. A. Montgomery, Jr., J. E. Peralta, F. Ogliaro, M. Bearpark, J. J. Heyd, E. Brothers, K. N. Kudin, V. N. Staroverov, T. Keith, R. Kobayashi, J. Normand, K. Raghavachari, A. Rendell, J. C. Burant, S. S. Iyengar, J. Tomasi, M. Cossi, N. Rega, J. M. Millam, M. Klene, J. E. Knox, J. B. Cross, V. Bakken, C. Adamo, J. Jaramillo, R. Gomperts, R. E. Stratmann, O. Yazyev, A. J. Austin, R. Cammi, C. Pomelli, J. W. Ochterski, R. L. Martin, K. Morokuma, V. G. Zakrzewski, G. A. Voth, P. Salvador, J. J. Dannenberg, S. Dapprich, A. D. Daniels, O. Farkas, J. B. Foresman, J. V. Ortiz, J. Cioslowski, D. J. Fox, Gaussian, Inc., Wallingford CT, **2010**.
[38] A. D. Becke, *J. Chem. Phys.* **1993**, *98*, 5648–5652.
[39] A. D. Becke, *J. Chem. Phys.* **1993**, *98*, 1372–1376.
[40] Y. Zhao, D. Truhlar, *Theor. Chem. Account* **2008**, *120*, 215–241.
[41] Y. Zhao, D. G. Truhlar, *Acc. Chem. Res.* **2008**, *41*, 157–167.
[42] A. V. Marenich, C. J. Cramer, D. G. Truhlar, *J. Phys. Chem. B* **2009**, *113*, 6378–6396.
[43] P. von Ragué Schleyer, F. Pühlhofer, *Org. Lett.* **2002**, *4*, 2873–2876.
[44] a) C. S. Wannere, P. von Ragué Schleyer, *Org. Lett.* **2003**, *5*, 865–868; b) C. S. Wannere, D. Moran, N. L. Allinger, B. Hess, Andes, L. J. Schaad, P. v. R. Schleyer, *Org. Lett.* **2003**, *5*, 2983–2986; c) C. S. Wannere, H. S. Rzepa, B. C. Rinderspacher, A. Paul, C. S. M. Allan, H. F. Schaefer, P. von Ragué Schleyer, *J. Phys. Chem. A* **2009**, *113*, 11619–11629.
[45] H. J. Dauben, J. D. Wilson, J. L. Layti, *J. Am. Chem. Soc.* **1968**, *90*, 811–813.
[46] T. A. Keith, R. F. W. Bader, *Chem. Phys. Lett.* **1993**, *210*, 223–231.
[47] M. K. Cyrański, T. M. Krygowski, A. R. Katritzky, P. von Ragué Schleyer, *J. Org. Chem.* **2002**, *67*, 1333–1338.
[48] a) P. von Ragué Schleyer, C. Maerker, A. Dransfeld, H. J. Jiao, N. Hommes, *J. Am. Chem. Soc.* **1996**, *118*, 6317–6318; b) Z. Chen, C. S. Wannere, C. Corminboeuf, R. Puchta, P. von Ragué Schleyer, *Chem. Rev.* **2005**, *105*, 3842–3888.
[49] C. Corminboeuf, T. Heine, G. Seifert, P. von Ragué Schleyer, J. Weber, *Phys. Chem. Chem. Phys.* **2004**, *6*, 273–276.
[50] a) J. Kruszewski, T. M. Krygowski, *Tetrahedron Lett.* **1972**, *13*, 3839–3842; b) T. M. Krygowski, *J. Chem. Inf. Comput. Sci.* **1993**, *33*, 70–78.
[51] F. De Proft, P. Geerlings, *Phys. Chem. Chem. Phys.* **2004**, *6*, 242–248.
[52] R. G. Parr, R. G. Pearson, *J. Am. Chem. Soc.* **1983**, *105*, 7512–7516.
[53] T. A. Koopmans, *Physica* **1934**, *1*, 104–113.
[54] M. Toganoh, H. Furuta, *J. Org. Chem.* **2010**, *75*, 8213–8223.
[55] There are several aromatic pathways in hexaphyrins. The classical conjugation pathway (CP) is based on the annulene model and passes through the iminic nitrogen atoms and bypasses the amino NH groups. Main macrocyclic conjugation pathways predicted by the bond resonance energies for various porphyrinoids support the annulene model: a) J. I. Aihara, *J. Phys. Chem. A* **2008**, *112*, 5305–5311. However, a recent analysis of the current pathways in twisted hexaphyrins showed that the current is split at the pyrrole rings, and the main current pathway does not always follow the inner non-hydrogenated C-N-C route: b) H. Fliegl, D. Sundholm, S. Taubert, F. Pichierri, *J. Phys. Chem. A* **2010**, *114*, 7153–7161.
[56] T. Koide, G. Kashiwazaki, M. Suzuki, K. Furukawa, M. C. Yoon, S. Cho, D. Kim, A. Osuka, *Angew. Chem.* **2008**, *120*, 9807–9811; *Angew. Chem. Int. Ed.* **2008**, *47*, 9661–9665.
[57] S. Shimizu, N. Aratani, A. Osuka, *Chem. Eur. J.* **2006**, *12*, 4909–4918.
[58] H. S. Rzepa, *Org. Lett.* **2008**, *10*, 949–952.
[59] Y. S. Xie, K. Yamaguchi, M. Toganoh, H. Uno, M. Suzuki, S. Mori, S. Saito, A. Osuka, H. Furuta, *Angew. Chem.* **2009**, *121*, 5604–5607; *Angew. Chem. Int. Ed.* **2009**, *48*, 5496–5499.
[60] M. Ishida, J-Y. Shin, Jong M. Lim, B. S. Lee, M.-C. Yoon, T. Koide, J. L. Sessler, A. Osuka, D. Kim, *J. Am. Chem. Soc.* **2011**, *133*, 15533–15544.
[61] M. Toganoh, H. Furuta, *J. Phys. Chem. A* **2009**, *113*, 13953–13963.
[62] In THF, the solvent used in the spectroscopic measurements, the activation energy barrier is predicted to be 7.5 kcal mol^{-1}, in very good agreement with the experimental value of 8 ± 1 kcal mol^{-1}.
[63] An exception is *meso*-hexakis(*2,6*-difluorophenyl)-substituted [28]hexaphyrin, which crystallized as a planar conformer from $CHCl_3$/*n*-heptane and as a Möbius conformer from 1,2-dichoroethane/ethanol.
[64] M. Mandado, M. J. González-Moa, R. A. Mosquera, *J. Comput. Chem.* **2007**, *28*, 127–136.
[65] E. Matito, M. Duran, M. Solà, *J. Chem. Phys.* **2005**, *122*, 014109.
[66] N. Otero, S. Fias, S. Radenković, P. Bultinck, A. M. Graña, M. Mandado, *Chem. Eur. J.* **2011**, *17*, 3274–3286.
[67] S. E. Wheeler, K. N. Houk, P. von Ragué Schleyer, W. D. Allen, *J. Am. Chem. Soc.* **2009**, *131*, 2547–2560.
[68] M. K. Cyrański, *Chem. Rev.* **2005**, *105*, 3773–3811.
[69] The *syn–anti* corrections applied to ISE values computed for [26]- and [28]hexaphyrin conformations are listed in the Supporting Information.
[70] Macrocyclic aromaticity in Hückel and Möbius conformers of several porphyrinoids was recently explored by means of the bond resonance energy: J. I. Aihara, H. Horibe, *Org. Biomol. Chem.* **2009**, *7*, 1939–1943.
[71] a) N. Sadlej-Sosnowska, *J. Phys. Org. Chem.* **2004**, *17*, 303–311; b) M. Alonso, C. Miranda, N. Martin, B. Herradón, *Phys. Chem. Chem. Phys.* **2011**, *13*, 20564–20574.
[72] J. I. Aihara, *J. Am. Chem. Soc.* **2006**, *128*, 2873–2879.
[73] R. G. Pearson, *Chemical Hardness*, Wiley, New York, **1997**.

Received: February 16, 2012
Revised: May 8, 2012
Published online: July 17, 2012

